Improving bulk $Ca_3Co_4O_9$ thermoelectric materials through Zr doping

M. A. Madre, Sh. Rasekh, M. A. Torres, J. C. Diez, A. Sotelo*

ICMA (Universidad de Zaragoza-CSIC), Dpto. de Ciencia y Tecnología de Materiales y Fluidos, C/María de Luna 3, E-50018, Zaragoza (Spain)

Abstract

$Ca_3Co_{4-x}Zr_xO_y$ polycrystalline ceramics with small Zr substitution have been prepared through the classical solid state method. XRD data have shown that all samples are only composed of $Ca_3Co_4O_9$ and $Ca_3Co_2O_6$ phases. Moreover, increasing Zr substitution up to 0.07, $Ca_3Co_2O_6$ phase content is decreased. Density measurements have revealed that all samples are very similar, with values around 74 % of the theoretical one. Electrical resistivity is decreased in Zr doped samples, with respect to the pure ones, while Seebeck coefficient is maintained practically unchanged. Both factors lead to power factor values around 0.33 mW/K^2m at 800 ºC in 0.07 Zr doped samples, which is about 65 % higher than the obtained for the undoped samples.

Keywords: Ceramics; Doping; Electric properties; Microstructure; Power factor

Corresponding author: A. Sotelo

e-mail: asotelo@unizar.es

Address: C/Maria de Luna, 3; 50018-Zaragoza; Spain

Tel: +34 976762617

Fax: +34 976761957

1. Introduction

Thermoelectric (TE) generation systems are able to directly transform, without any mobile element, temperature gradients to useful electrical power through the Seebeck effect. The efficiency of such process in these materials is evaluated through the dimensionless figure-of-merit, ZT, which is defined as $TS^2/\rho\kappa$, where S is the Seebeck coefficient (or thermopower), ρ the electrical resistivity, κ the thermal conductivity, and T is the absolute temperature [1]. Moreover, in this expression, the electrical part, S^2/ρ, is called power factor, PF. Nowadays, these thermoelectric materials are regarded as very attractive to recover waste heat produced in classical energy transforming systems [2], increasing their efficiency and decreasing CO_2 release. As a consequence, they can help in the fight against global warming.

Most of the practical applications of these thermoelectric systems are based on intermetallic materials, such as Bi_2Te_3 [3,4], with high ZT values at relatively low temperatures, being degraded and/or oxidized when working at high temperatures [5]. On the other hand, the discovery of high thermoelectric properties in $Na_2Co_2O_4$ ceramic materials [6] overcame these limitations. The subsequent research on the CoO-based family led to the discovery and optimization of new members, such as $Ca_3Co_4O_9$ [7,8] and $Bi_2AE_2Co_2O_x$ (AE: alkaline earth) [9-12], with high thermoelectric properties and working temperatures.

Crystallographic studies performed on those Co-based materials have demonstrated that they possess large structural anisotropy [13], reflected in a preferential crystal growth along the ab planes. The formation of plate-like grains has been exploited to align them using different methods to reach

macroscopic properties comparable to single crystals ones. Among these methods, it can be highlighted hot uniaxial pressing [14], spark plasma sintering [15], or laser floating zone melting (LFZ) [16]. On the other hand, in spite of the high performances obtained in materials processed through these techniques, their use for mass production still remains a problem. In order to avoid the drawbacks of these techniques, other easily scalable processes, as synthesis methods [17,18] or doping [19,20] have been studied to produce high performance materials.

The aim of this work is to study the effect of Zr substitution for Co in the $Ca_3Co_4O_y$ ceramics prepared through the classical solid state route. The structural and microstructural modifications will be studied and related with the thermoelectric performances.

2. Experimental

$Ca_3Co_{4-x}Zr_xO_y$ polycrystalline ceramic materials, with x = 0.00, 0.01, 0.05, 0.07, 0.10, and 0.15, were prepared by the conventional solid state route using $CaCO_3$ (Panreac, 98 + %), Co_2O_3 (Aldrich, 98 + %), and ZrO_2 (Aldrich, 99 %) commercial powders as starting materials. Adequate proportions of each powder were well mixed and ball milled at 300 rpm for 30 minutes, in water media. The slurry was totally dried using infrared radiation, followed by a manual milling, and a two-steps thermal treatment at 750 and 800 ºC for 12h, with an intermediate manual grinding to decompose the calcium carbonate [8]. The resulting powders were uniaxially pressed in form of pellets (3 x 3 x 14 mm^3) at 400 MPa, perpendicularly to their long axis, followed by a sintering procedure at 910 ºC for 24 h with a final furnace cooling.

Powder X-ray diffraction (XRD) patterns have been recorded to identify the different phases in the sintered materials. Data have been collected with 2θ ranging between 5 and 60 degrees, using a Rigaku D/max-B X-ray powder diffractometer working with Cu Kα radiation.

Microstructural observations were performed on longitudinal surfaces, using a Field Emission Scanning Electron Microscope (FESEM, Carl Zeiss Merlin). Chemical qualitative analysis of the different phases has been made with an energy dispersive spectrometry (EDS) device. Moreover, apparent density measurements have been performed on several samples for each composition after sintering, using 4.677 g/cm^3 as theoretical density [21].

Electrical resistivity and Seebeck coefficient were simultaneously determined by the standard dc four-probe technique, along the long axis of pellets, using a LSR-3 system (Linseis GmbH) between 50 and 800 ºC. Power Factor has been calculated, using the electrical resistivity and Seebeck coefficient data, to determine the samples performances. All these thermoelectric properties have been compared with the results of undoped samples, and with the best reported in the literature.

3. Results and discussion

Powder XRD patterns of some of the $Ca_3Co_{4-x}Zr_xO_y$ samples are shown in Fig. 1 (from 5 to 40º for the sake of clarity). These graphs illustrate the general evolution of samples with Zr content. At a first sight, it can be observed that all the samples show very similar diffraction patterns. In all samples the most intense peaks have been associated to the thermoelectric $Ca_3Co_4O_9$ phase, identified by their reflection planes in Fig. 1a, in agreement with previous data

[22]. On the other hand, some minor peaks, corresponding to the $Ca_3Co_2O_6$ phase [22], appear (identified by * in Fig 1a). Moreover, the intensity of the secondary phase peaks is reduced when Zr is added until 0.07 Zr, slightly increasing for higher content. This is a clear indication that small amounts of Zr increase the $Ca_3Co_4O_9$ phase stability. On the other hand, no other secondary phases have been identified in the XRD diagrams pointing out to the Zr incorporation into the $Ca_3Co_4O_9$ crystal structure.

SEM micrographs performed on representative surfaces of some of the samples are presented in Fig. 2. In the figure, it can be clearly seen that all samples are composed by randomly oriented plate-like grains with similar sizes. Moreover, as identified through EDS, major phase is the thermoelectric $Ca_3Co_{4-x}Zr_xO_y$ one (grey contrast) in all samples. Zr-free $Ca_3Co_2O_6$ secondary phase (#1) can be also seen in Fig. 2a as a slightly darker grey contrast and different grain shape. The content of this phase in the samples is decreased when Zr is added up to 0.07, being maintained or slightly increased for higher Zr addition. This microstructural evolution clearly agrees with the XRD data previously discussed. Finally, for high Zr content, $\geq$ 0.10, a dark grey contrast appears (#2) corresponding to CaO. Moreover, a white one is also appearing in noticeable content (#3), identified as $CaZrO_3$. These phases have not been found in the XRD patterns due to their small amount. Other interesting observation made in these micrographs is that the samples porosity is not appreciably modified with Zr addition. This effect can be associated to the relatively low thermal stability of this phase (maximum stability temperature 926 ºC), compared with the melting point of this CaO-CoO system (around 1350 ºC) [23].

In order to confirm the SEM observations about the negligible effect of Zr addition on the porosity of samples, apparent density measurements have been made in all samples. At least five samples of each composition were determined for three times to decrease the errors associated to their measurement. The density values showed a good reproducibility, with a standard error of around $\pm$ 0.01 g/cm^3 in all samples, and very similar mean values for all samples, around 3.45 g/cm^3, which corresponds to about 74 % of the $Ca_3Co_4O_9$ phase theoretical density. These results clearly agree with the SEM images previously discussed which showed no evident effect of Zr addition on the porosity of samples.

The temperature dependence of electrical resistivity, as a function of the Zr content, is shown in Fig. 3. The ρ (T) curves show a decrease of resistivity when Zr is added, in the whole measured temperature range, when compared to the undoped samples. Moreover, in a general view the curves show a semiconducting ($d\rho/dT < 0$) behaviour, from room temperature to around 400 ºC in all cases, changing to a metallic one ($d\rho/dT > 0$) at higher temperatures. On the other hand, for Zr content $\geq$ 0.05, the semiconducting part of the curves is modified and a metallic behaviour region can be found below 200 ºC, while the semiconducting one is limited to temperatures between 200 and 400 ºC. The decrease of resistivity found in these samples can be associated to the partial substitution of Co^{3+} and Co^{4+} from the conducting layer by Zr^{4+} [24], and to the increase of the thermoelectric phase content. The lowest resistivity values in the whole measured temperature range have been measured in 0.07 Zr-doped samples (12.6, and 15.0 mΩ.cm at room temperature and 800 ºC, respectively), which are lower than the obtained for hot-pressed textured samples (33, and 40

mΩ.cm) [14]. On the other hand, they are higher than the measured in textured samples produced through SPS (5, and 6 mΩ.cm) [25], or by more complex preparation methods (10.7, and 13.5 mΩ.cm) [26,27]. It should be highlighted that all these reported results have been obtained in higher density samples than the produced in this work, clearly indicating the electrical resistivity improvement produced by Zr doping.

Fig. 4 shows the variation of the Seebeck coefficient with temperature, as a function of Zr substitution. In the graph, it can be observed that the sign of the Seebeck coefficient is positive, independently of temperature, indicating that the conduction mechanism is produced by holes. Moreover, it increases when the temperature is raised, with very similar values and behaviour for all the samples, indicating that Zr doping does not affect, in a great extent, the $Ca_3Co_4O_9$ conduction band [28]. Furthermore, the fact that this increase is nearly linear can be associated with a typical behaviour of a metallic compound or a semiconductor in the saturation region [29]. The maximum values at room temperature and 800 ºC (135, and 235 μV/K, respectively) are significantly higher than the values obtained for $Ca_3Co_4O_9$ samples consolidated by spark plasma sintering (125, and 165 μV/K) [25], or doped and sintered specimens (≤ 160, and ≤ 200 μV/K) [30]. Moreover, they are comparable to the highest reported so far in $Ca_3Co_4O_9$/Ag composite materials subjected to a two steps thermal treatment (135, and 240 μV/K) [31].

The thermoelectric performances of these materials have been evaluated through the power factor, calculated using the electrical resistivity and Seebeck coefficient data. Its evolution as a function of temperature and Zr content is presented in Fig. 5. When considering PF values at around room temperature, it

can be clearly seen that all the Zr-doped samples possess higher PF values than the undoped ones. The values are increased with Zr content until they reach the maximum (0.15 mW/K^2.m) for 0.07 Zr substitution, decreasing for higher content. PF is increased with temperature in all samples, reaching the maximum measured values at 800 ºC (around 0.33 mW/K^2.m) in the 0.07 Zr substituted samples, which are 65 % higher than the measured in undoped samples. This value is slightly higher than the obtained in samples produced by classical solid state method and consolidated through spark plasma sintering (0.32 mW/K^2.m) [32], but lower than samples produced by autocombustion and textured with SPS (0.50 mW/K^2.m) measured along the *ab* direction [25]. Moreover, they are higher than the determined in rare earth doped materials (0.27 mW/K^2.m) [33]. On the other hand, they are still lower than the obtained in samples produced through more complex methods (0.43 mW/K^2.m) [15,21,26,27,31]. The important raise obtained in PF through Zr doping is mainly associated to the drastic decrease of electrical resistivity, without significant modification of Seebeck coefficient. Moreover, it is worth to mention that these values have been obtained in samples with relatively low density and random grain orientation.

All these data point out that Zr doping is adequate to improve the thermoelectric performances of $Ca_3Co_4O_9$ ceramics, which can be further raised though processes increasing density and/or aligning the grains, approaching these materials to their practical applications.

4. Conclusions

This paper demonstrates that Zr substitution for Co in $Ca_3Co_4O_9$ materials improves their thermoelectric performances. Zr substitution up to 0.07 decreases the $Ca_3Co_2O_6$ secondary phase content, slightly increasing for further substitution. The microstructural modifications are reflected in a decrease of electrical resistivity, when compared with the undoped samples, without drastic modification of Seebeck coefficient. The optimal Zr substitution has been determined through the PF values at 50 and 800 ºC, which is maximum for 0.07 Zr samples. The highest PF values at 800 ºC are about 65 % higher than the obtained for the undoped samples. Moreover, they are slightly higher than the values obtained in typical samples produced by spark plasma sintering or through the classical solid state method.

Acknowledgements

The authors wish to thank the Gobierno de Aragón-FEDER (Grupos de Investigacion Consolidados T12 and T87) and MINECO-FEDER (MAT2013-46505-C3-1-R) for financial support. Authors would like to acknowledge the use of Servicio General de Apoyo a la Investigación-SAI, Universidad de Zaragoza.

References

[1] Rowe DM, ed. Thermoelectrics handbook: macro to nano. 1st ed. CRC 1_3–1_7; 2006, Boca Raton (FL): CRC Press; 2006.

[2] Mahan G, Sales B, Sharp J. Thermoelectric materials: new approaches to an old problem, Phys Today. 1997;50:42–47.

[3] Santamaria JM, Alkorta J, Sevillano JG. Mechanical properties of bismuth telluride (Bi_2Te_3) processed by high pressure torsion (HPT). Bol Soc Esp Ceram V. 2013;52:137–142.

[4] Wang HC, Bahk J-H, Kang C, et al. Right sizes of nano and microstructures for high-performance and rigid bulk thermoelectrics. P Natl Acad Sci USA. 2014;111:10949–10954.

[5] Elsheikh MH, Shnawah DA, Sabri MFM, et al. A review on thermoelectric renewable energy: principle parameters that affect their performance. Renew Sust Energ Rev. 2014;30:337–355.

[6] Terasaki I, Sasago Y, Uchinokura K. Large thermoelectric power in $NaCo_2O_4$ single crystals. Phys Rev B. 1997;56:12685–12687.

[7] Huang Y, Zhao B, Fang J, et al. Tunning of microstructure and thermoelectric properties of $Ca_3Co_4O_9$ ceramics by high-magnetic-field sintering. J Appl Phys. 2011;110:123713.

[8] Constantinescu G, Rasekh S, Torres MA, et al. Effect of Sr substitution for Ca on the $Ca_3Co_4O_9$ thermoelectric properties. J Alloys Compds. 2013;577:511–515.

[9] Shen JJ, Liu XX, Zhu TJ, et al. Improved thermoelectric properties of La-doped $Bi_2Sr_2Co_2O_9$-layered misfit oxides. J Mater Sci. 2009;44:1889–1893.

[10] Rasekh Sh, Constantinescu G, Torres MA, et al. Growth rate effect on microstructure and thermoelectric properties of melt grown $Bi_2Ba_2Co_2O_x$ textured ceramics. Adv Appl Ceram. 2012;111:490–494.

[11] Luo XG, Jing YC, Chen H, et al. Intergrowth and thermoelectric properties in the Bi-Ca-Co-O system. J Cryst Growth. 2007;308:309–313.

[12] Madre MA, Rasekh, Diez JC, et al. New solution method to produce high performance thermoelectric ceramics: A case study of Bi-Sr-Co-O. Mater Lett. 2010;64:2566–2568.

[13] Miyazaki Y. Crystal structure and thermoelectric properties of the misfit-layered cobalt oxides. Solid State Ionics. 2004;172:463–467.

[14] Wang H, Sun X, Yan X, et al. Fabrication and thermoelectric properties of highly textured $Ca_9Co_{12}O_{28}$ ceramic. J Alloys Compds. 2014;582:294–298.

[15] Noudem JG, Kenfaui D, Chateigner D, et al. Toward the enhancement of thermoelectric properties of lamellar $Ca_3Co_4O_9$ by edge-free spark plasma texturing. Scr Mater. 2012;66:258–260.

[16] Rasekh Sh, Ferreira NM, Costa FM, et al. Development of a new thermoelectric $Bi_2Ca_2Co_{1.7}O_x$ + $Ca_3Co_4O_9$ composite. Scr Mater. 2014;80:1–4.

[17] Sotelo A, Rasekh Sh, Torres MA, et al. Preparation of high performances $Bi_2Sr_2Co_{1.8}O_x$ thermoelectric materials from nanosized precursors. Adv Appl Ceram. 2017[cited 2017 June 27];[9 p.]. DOI: 10.1080/17436753.2017.1339491

[18] Sotelo A, Torres MA, Rasekh Sh, et al. Effect of precursors on the microstructure and electrical properties of $Bi_2Ba_2Co_2O_x$. J Aust Ceram Soc. 2017[cited 2017 June 27];[8 p.]. DOI: 10.1007/s41779-017-0070-6

[19] Sun N, Dong ST, Zhang BB, et al. Intrinsically modified thermoelectric performance of alkaline-earth isovalently substituted $[Bi_2AE_2O_4][CoO_2]y$ single crystals. J Appl Phys. 2013;114:043705.

[20] Delorme F, Martin CF, Marudhachalam P, et al. Effect of Ca substitution by Sr on the thermoelectric properties of $Ca_3Co_4O_9$ ceramics. J Alloys Compds. 2011;509:2311–2315.

[21] Madre MA, Costa FM, Ferreira NM, et al. Preparation of high-performance $Ca_3Co_4O_9$ thermoelectric ceramics produced by a new two-step method. J Eur Ceram Soc. 2013;33:1747–1754.

[22] Woermann E, Muan A. Phase equilibria in the system CaO–cobalt oxide in air. J Inorg Nucl Chem. 1970;32:1455–1459.

[23] Diez JC, Torres MA, Rasekh Sh, et al. Enhancement of $Ca_3Co_4O_9$ thermoelectric properties by Cr for Co substitution. Ceram Int. 2013;39:6051–6056.

[24] Pinitsoontorn S, Lerssongkram N, Keawprak N, et al. Thermoelectric properties of transition metals-doped $Ca_3Co_{3.8}M_{0.2}O_{9+\delta}$ (M = Co, Cr, Fe, Ni, Cu and Zn). J Mater Sci Mater Electron. 2012;23:1050–1056.

[25] Wu NY, Holgate TC, Nong NV, et al. High temperature thermoelectric properties of $Ca_3Co_4O_{9+\delta}$ by auto-combustion synthesis and spark plasma sintering. J Eur Ceram Soc. 2014;34:925–931.

[26] Sotelo A, Rasekh S, Torres MA, et al. Effect of synthesis methods on the $Ca_3Co_4O_9$ thermoelectric ceramic performances. J Solid State Chem. 2015;221:247–254.

[27] Sotelo A, Costa FM, Ferreira NM, et al. Tailoring $Ca_3Co_4O_9$ microstructure and performances using a transient liquid phase sintering additive. J Eur Ceram Soc. 2016;36:1025–1032.

[28] Rasekh Sh, Torres MA, Constantinescu G, et al. Effect of Cu by Co substitution on $Ca_3Co_4O_9$ thermoelectric ceramics. J Mater Sci Mater Electron. 2013;24:2309–2314.

[29] Constantinescu G, Rasekh Sh, Torres MA, et al. Thermoelectric doping effect in $Ca_3Co_{4-x}Ni_xO_9$ ceramics. Bol Soc Esp Ceram V. 2015;54:21–27.

[30] Abdellahi M, Bahmanpour M, Bahmanpour M. Modeling Seebeck coefficient of $Ca_{3-x}M_xCo_4O_9$ (M = Sr, Pr, Ga, Ca, Ba, La, Ag) thermoelectric ceramics. Ceram Int. 2015;41:345–352.

[31] Kahraman F, Madre MA, Rasekh Sh, et al. Enhancement of mechanical and thermoelectric properties of $Ca_3Co_4O_9$ by Ag addition. J Eur Ceram Soc. 2015;35:3835–3841.

[32] Kenfaui D, Bonnefont G, Chateigner D, et al. $Ca_3Co_4O_9$ ceramics consolidated by SPS process: Optimisation of mechanical and thermoelectric properties. Mater Res Bull. 2010;45:1240–1249.

[33] Rasekh Sh, Constantinescu G, Torres MA, et al. Thermoelectric properties of rare earth doped $Ca_{3-x}RE_xCo_4O_9$ (RE = Dy, Er, Gd, and Tb; x=0, 0.01, 0.03, and 0.05). J Electroceram. 2014;32:376–382.

Figure captions:

Figure 1. Powder X-ray diffraction patterns obtained for the $Ca_3Co_{4-x}Zr_xO_y$ samples; x = 0.00 (a); 0.05 (b); 0.07 (c); and 0.10 (d). The diffraction planes indicate the $Ca_3Co_4O_9$ phase peaks and the * the $Ca_3Co_2O_6$ ones.

Figure 2. Representative SEM micrographs performed on the surface of $Ca_3Co_{4-x}Zr_xO_y$ samples; x = 0.00 (a); 0.05 (b); 0.07 (c); and 0.10 (d). Grey contrast corresponds to the $Ca_3Co_{4-x}Zr_xO_y$ phase; slightly darker grey (#1) to $Ca_3Co_2O_6$, and the darkest grey (#2) to CaO. Small white particles (#3) found in the higher Zr-substituted samples corresponds to $CaZrO_3$.

Figure 3. Temperature dependence of electrical resistivity, as a function of the Zr content in $Ca_3Co_{4-x}Zr_xO_y$ samples, for x = 0.00 (▲); 0.01 (■); 0.05 (◆); 0.07 (▼); 0.10 (◣); and 0.15 (◢).

Figure 4. Temperature dependence of Seebeck coefficient as a function of Zr substitution in $Ca_3Co_{4-x}Zr_xO_y$ samples, for x = 0.00 (▲); 0.01 (■); 0.05 (◆); 0.07 (▼); 0.10 (◣); and 0.15 (◢).

Figure 5. Temperature dependence of the power factor as a function of Zr substitution in $Ca_3Co_{4-x}Zr_xO_y$ samples, for x = 0.00 (▲); 0.01 (■); 0.05 (◆); 0.07 (▼); 0.10 (◣); and 0.15 (◢).

Figure 1

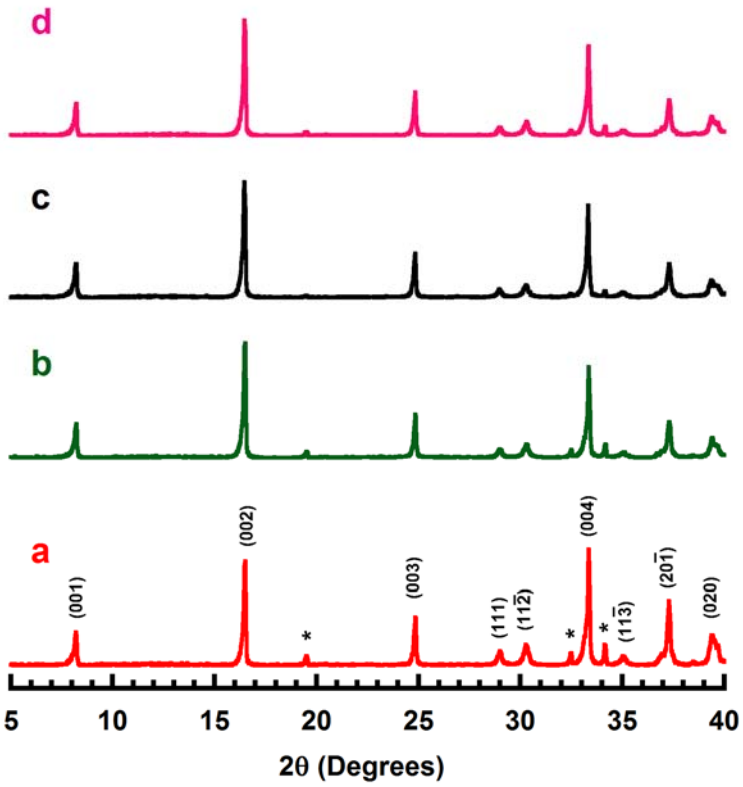
d
c
b
a
(001)
(002)
(003)
(111)
(11$\bar{2}$)
(004)
(11$\bar{3}$)
(20$\bar{1}$)
(020)
*
5
10
15
20
25
30
35
40
2θ (Degrees)

Figure 2

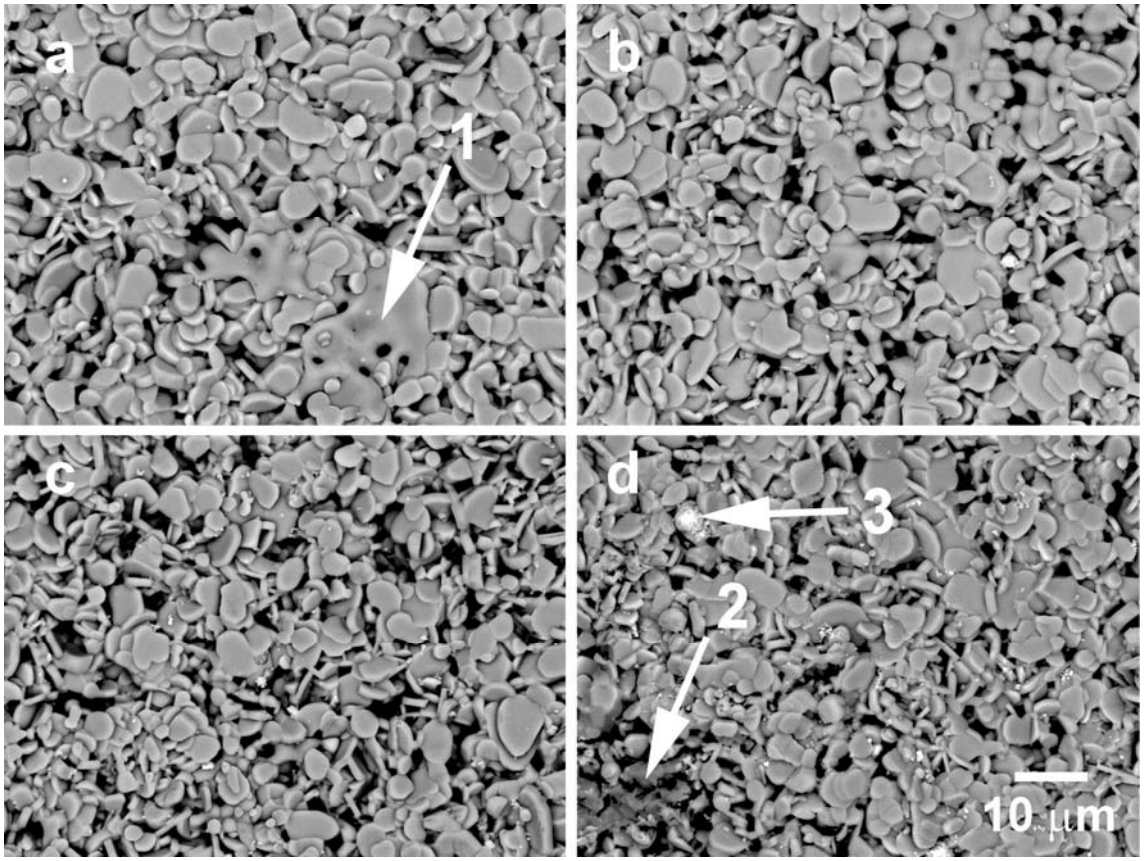

Figure 3

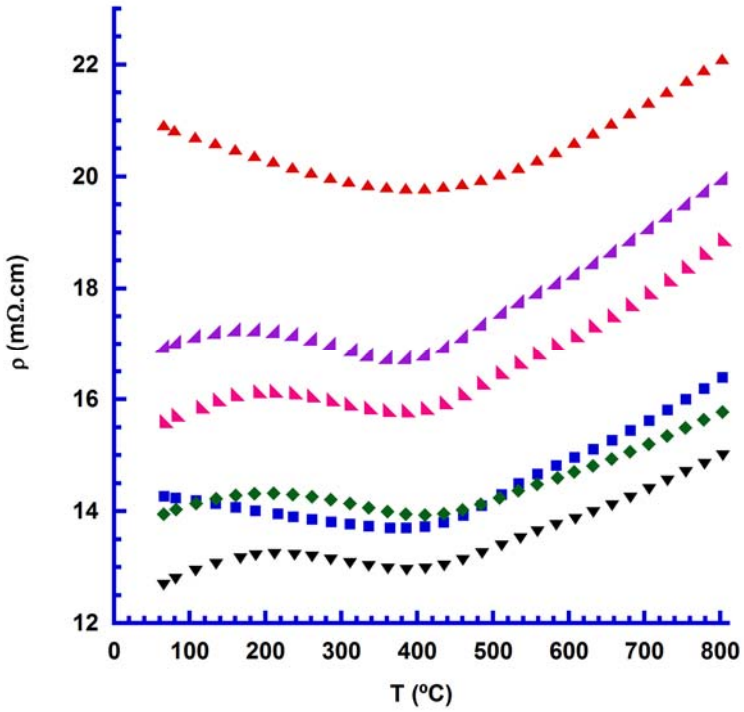

Figure 4

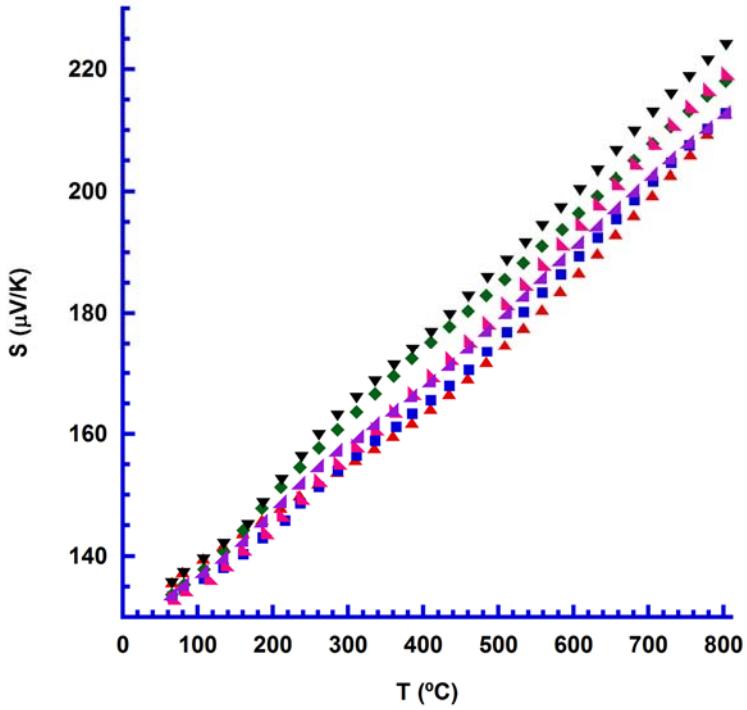

Figure 5

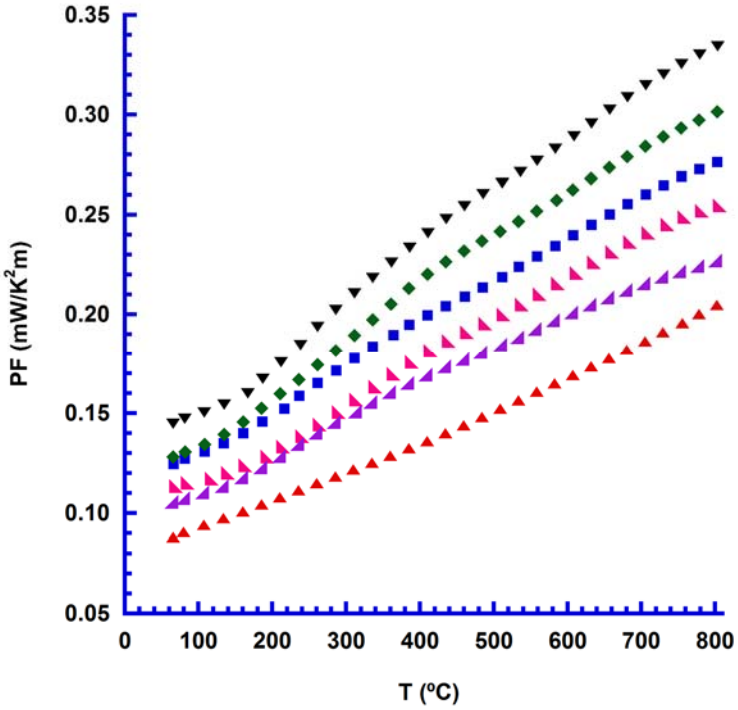
0.35
0.30
0.25
0.20
0.15
0.10
0.05
PF (mW/K²m)
0
100
200
300
400
500
600
700
800
T (ºC)